Observation of Antiferromagnetic Domains in Epitaxial Thin Films

A. Scholl,[1]* J. Stöhr,[2] J. Lüning,[2] J. W. Seo,[4,3] J. Fompeyrine,[3] H. Siegwart,[3] J.-P. Locquet,[3] F. Nolting,[1] S. Anders,[1] E. E. Fullerton,[2] M. R. Scheinfein,[5] H. A. Padmore[1]

Antiferromagnetic domains in an epitaxial thin film, $LaFeO_3$ on $SrTiO_3$(100), were observed using a high-spatial-resolution photoelectron emission microscope with contrast generated by the large x-ray magnetic linear dichroism effect at the multiplet-split *L* edge of Fe. The antiferromagnetic domains are linked to 90° twinned crystallographic regions in the film. The Néel temperature of the thin film is reduced by 70 kelvin relative to the bulk material, and this reduction is attributed to epitaxial strain. These studies open the door for a microscopic understanding of the magnetic coupling across antiferromagnetic-ferromagnetic interfaces.

The current interest in magnetism is largely based on atomically engineered thin film structures, owing to the interesting physics of these materials and their technological use in the magnetic storage industry (*1*). An important and scientifically challenging class of materials is antiferromagnetic (AFM) thin films, which are extensively used in exchange bias applications (*2*). Exchange bias is used to magnetically pin a ferromagnetic layer to an adjacent antiferromagnet, thereby acting as a reference layer in a magnetic device. This technologically important effect is still poorly understood because of the inability of traditional techniques to spatially determine the microscopic magnetic structure of the AFM thin film. Although the AFM domain structure in bulk single crystals has been studied since the late 1950s (*3, 4*) little is known about the domain structure in thin films. For example, in well-annealed bulk NiO the typical domain size is in the range of 0.1 to 1 mm (*3, 5*), whereas in epitaxial NiO films the domain size has been estimated to be less than 50 nm (*6*). This size is below the spatial resolution of neutron diffraction topography (about 70 μm), x-ray diffraction topography (1 to 2 μm) (*4*), and the fundamental resolution limit (about 0.2 μm) set by diffraction for optical (*3, 5*) and nonlinear optical (*7*) techniques. Here we demonstrate the ability of x-ray spectromicroscopy to image the magnetic structure of AFM thin films with high spatial resolution, which is a necessary step toward a better understanding of exchange bias.

In particular, first images of the AFM domain structure in a thin film, $LaFeO_3$, grown epitaxially on $SrTiO_3$, are reported. They were obtained with x-ray magnetic linear dichroism (XMLD) spectromicroscopy (*8, 9*), using a new facility that combines a high-flux-density soft x-ray beam line with a high spatial resolution (20 nm) photoelectron emission microscope (PEEM) (*10*). Like PEEM spectromicroscopy of ferromagnets by use of circular dichroism (*11*), the XMLD-PEEM technique offers high spatial resolution in conjunction with elemental and chemical specificity and surface sensitivity (~2 nm sampling depth) (*9*).

The sample studied was a thin 40-nm $LaFeO_3$ film deposited on an asymmetric $SrTiO_3$(100) (**a** = 3.905 Å) bicrystal, where two (100) crystals were joined macroscopically at (110) and (010) faces, leading to a 45° rotation of the lattice around the surface normal. The $LaFeO_3$ film was grown in an oxide molecular beam epitaxy (MBE) system by means of a block-by-block growth method (*12*) at 750°C under a beam of atomic oxygen and a partial O_2 pressure of 5×10^{-6} torr. This method has been shown to yield high-quality epitaxial films (*13*). The lattice parameters of bulk orthorhombic $LaFeO_3$ are **a** = 5.557 Å, **b** = 5.5652 Å, and **c** = 7.8542 Å (*14*), with the antiferromagnetic vector $\vec{A}$ pointing along the **a** axis (*15*). Plane-view electron diffraction and conventional transmission electron microscope (TEM) analysis of the epitaxial $LaFeO_3$ bicrystal, performed with a 200-kV JEOL 2010 microscope, showed that both macroscopic parts consist of four microscopic crystallographic domains characterized by orientations of the $LaFeO_3$ **c** axis along the [100], [-100], [010], and [0-10] directions in the $SrTiO_3$ surface plane. The **a** and **b** axes are canted by 45° out of the surface plane. A rectangular network of dislocations was observed, and their average distances were used to obtain the in-plane (pseudo-cubic) lattice parameters **c*** = 3.920 Å, **b*** = 3.938 Å, whereas the out-of-plane lattice parameter **a*** = 3.947 Å was obtained by means of x-ray diffraction.

The samples were studied with x-ray absorption spectroscopy and spectromicroscopy (*10, 16*). The focused, linearly polarized x-rays are incident on the sample at an angle of 30° from the surface, with the electric field vector $\vec{E}$ oriented parallel to the surface. The all-electrostatic PEEM2 microscope images low-energy secondary photoelectrons from the sample with magnification onto a phosphor screen that is read by a charge-coupled device (CCD) camera. The spatial resolution of PEEM2 is limited to 20 nm by chromatic aberrations. In order to avoid charging effects, the insulating $LaFeO_3$ sample was coated with a 1.5-nm Cu layer in the PEEM preparation chamber.

Our experiments make use of the large XMLD effect previously observed in α-Fe_2O_3 (*17*). In both α-Fe_2O_3 and $LaFeO_3$, the Fe^{3+} ion has a $3d^5$, high-spin $S = 5/2$ ground state and an approximately octahedral environment. The *L* edge x-ray absorption fine structure for $LaFeO_3$ recorded by total electron yield detection (Fig. 1) is nearly identical to the experimental and theoretical spectra for α-Fe_2O_3 (*17*). For octahedral symmetry, there is no conventional linear (charge) dichroism, and the temperature and polarization dependence of the Fe *L* edge resonance intensity is given by (*6, 18*)

$$I(\theta,T) = a + b\,(3\cos^2\theta - 1)\langle M^2\rangle_T \quad (1)$$

where the first term is a constant and the second XMLD term depends on the x-ray larization through the angle θ between $\vec{E}$ and the magnetic axis $\vec{A}$ and on temperature (*T*) through the magnetic moment $\langle M^2\rangle_T$, which vanishes above the Néel temperature. Here we have neglected a smaller spin-spin correlation term

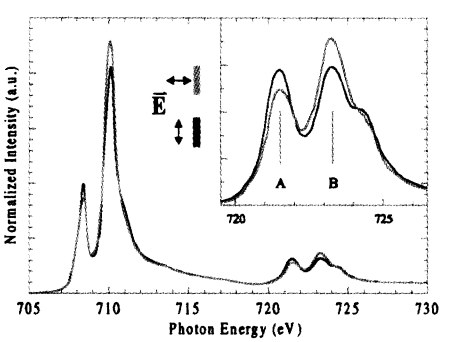

Fig. 1. Total electron yield of Fe *L* edge XMLD spectra for a 26-nm-thick film of $LaFeO_3$ grown on $SrTiO_3$(100). The spectra have been corrected for saturation effects and incomplete polarization alignment effects and correspond to alignment of the $\vec{E}$ vector along and perpendicular to the surface normal. a.u., arbitrary units.

[1]Advanced Light Source, 1 Cyclotron Road, Lawrence Berkeley National Laboratory, Berkeley, CA 94720, USA. [2]IBM Research Division, Almaden Research Center, 650 Harry Road, San Jose, CA 95120, USA. [3]IBM Research Division, Zürich Research Laboratory, CH-8803 Rüschlikon, Switzerland. [4]Institut de Physique, University of Neuchâtel, CH-2000 Neuchâtel, Switzerland. [5]Department of Physics and Astronomy, Arizona State University, Tempe, AZ 85287–1504, USA.

*To whom correspondence should be addressed. E-mail: a_scholl@lbl.gov

(*18*). The angle-dependent XMLD effect is due to a preferential orientation of the antiferromagnetic axis $\vec{A}$. In particular, peak A at 721.5 eV is larger than peak B at 723.2 eV (Fig. 1 inset) for $\vec{E} \perp \vec{A}$ and smaller for $\vec{E} \parallel \vec{A}$. From a careful study of the angular dependence of the XMLD effect in $LaFeO_3$ film on $SrTiO_3$ substrates with various symmetry (*19*), we determined that for $LaFeO_3/SrTiO_3(100)$, $\vec{A}$ is inclined 45° from the surface normal. The spectroscopy measurements do not reveal any preferential azimuthal orientation of $\vec{A}$ because they average over the fourfold symmetric domains.

The AFM domains can be directly observed by combining XMLD spectroscopy with PEEM microscopy; that is, by dividing a PEEM image acquired at 723.2 eV (peak B) by one obtained at 721.5 eV (peak A). The resultant image (Fig. 2) was recorded across the bicrystal junction (crystal orientation is indicated by arrows) and reveals striking AFM domains on the right side of the junction and a uniform gray shade on the left side. The strong magnetic contrast on the right side arises from magnetic domains with an in-plane projection of $\vec{A}$ parallel (white) and perpendicular (black) to the horizontal $\vec{E}$ vector. On the left side, the domains cannot be distinguished because $\vec{E}$ has an equal 45° projection onto the two orientations of $\vec{A}$. Because in our experimental geometry $\vec{E}$ lies in the surface plane, we cannot distinguish domains whose axis $\vec{A}$ is rotated by 180° about the surface normal. Thus we only observed two of the four antiferromagnetic domains that have to exist by symmetry. A plan-view TEM image of the bicrystal is shown in the lower right inset of Fig. 2. The imaging conditions of this dark field image were chosen so that domains with orthogonal orientation of the **c** axis gave rise to bright or dark contrast. The contrast is also affected by the presence of dislocations. The close correspondence between the domain sizes in the PEEM and TEM images suggests that the AFM domains are seeded by the structural domains so that the projection of the magnetic axis $\vec{A}$ is either parallel or perpendicular to the crystallographic **c** axis. The relationship between crystal structure and the four antiferromagnetic domains is summarized in the lower left inset of Fig. 2.

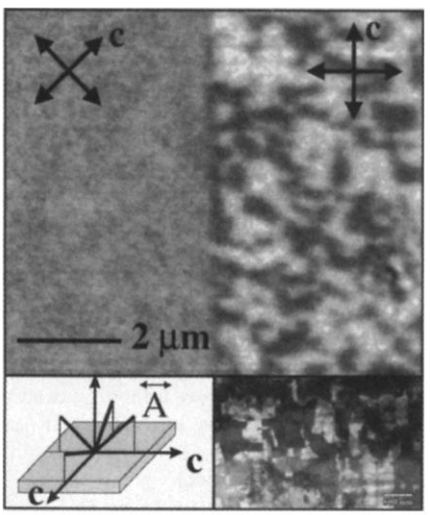

Fig. 2. XMLD image obtained by division of images taken at photon energies 723.2 eV (peak B) and 721.5 eV (peak A) for the bicrystal sample. Arrows indicate the orientation of the crystallographic **c** axes. Photon polarization $\vec{E}$ is horizontal. The bottom left inset illustrates the relation between magnetic and crystallographic structure; the bottom right inset shows a plan-view TEM image of the bicrystal with image contrast arising from regions with orthogonal **c** axes.

In a collection of XMLD images (Fig. 3) obtained at different temperatures between 290 and 550 K, the image contrast is strongly reduced at elevated temperatures and it is completely reversible upon cooling to room temperature, indicating that, within the studied temperature range, the magnetic state of the sample is not affected by chemical or diffusive processes at the sample surface. This is also supported by the unchanged x-ray absorption fine structure recorded before and after the temperature series. The quantitative XMLD image contrast is also plotted (Fig. 3), measured for two temperature cycles. According to Eq. 1, the XMLD contrast is a measure of the square of the AFM moment $\langle M^2 \rangle_T$. We have fitted the data in Fig. 3 with the shown solid line, using the exact expression for $\langle M^2 \rangle_T$ in terms of $\langle M \rangle_T$ (*20, 21*). $\langle M \rangle_T$ has been approximated following mean field theory with $S = 5/2$ (*21*). Data and fit are normalized to 1 at 0 K. From the fit, we obtain the Néel temperature (T_N) = 670 ± 10 K for the thin film. This value is significantly reduced relative to that of bulk $LaFeO_3$, with T_N = 740 K (Fig. 3, arrow) (*22*). The temperature dependence shown in Fig. 3 clearly establishes the AFM origin of the image contrast and indicates that crystallographic distortions of the octahedral Fe environment make only a negligible contribution.

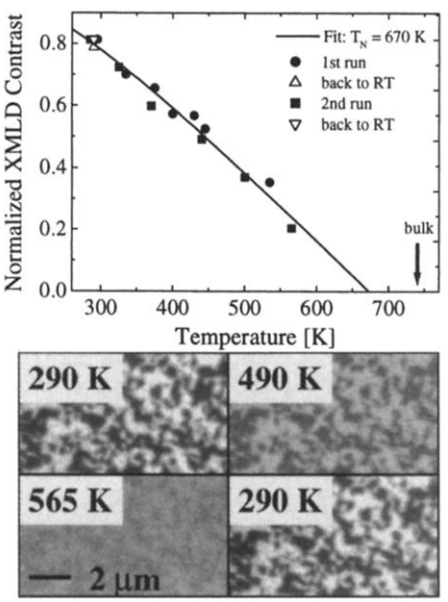

Fig. 3. Temperature dependence of the AFM domain contrast. A fit using $\langle M^2 \rangle$ mean field theory, resulting in T_N = 670 K, is shown. The data and fit are normalized to 1 at 0 K.

The reduced Néel temperature is unlikely to be due to a finite size effect. Both the film thickness and the size of the crystallographic domains are considerably larger than the dimensions (about 10 nm) below which finite size effects have been found in AFM oxide films such as NiO and CoO (*18, 23*). Instead, we attribute the reduced Néel temperature to epitaxial strain. In mean field theory, the Néel temperature in $LaFeO_3$ is proportional to both the exchange coupling constant J and to the Fe spin S according to $S(S + 1)$. Epitaxial strain affects J through changes in the Fe-O-Fe superexchange angle (*24*), and it can reduce the high spin state $S = 5/2$ through crystal field effects associated with distortions of the FeO_6 octahedra. For our $LaFeO_3$ thin film, x-ray diffraction and TEM detect an in-plane lattice contraction along the **c** axis of about 0.2% as compared to bulk $LaFeO_3$ with a comparable in-plane expansion perpendicular to **c**. The out-of-plane lattice expansion is even larger (0.4%). With two lattice parameters larger than the bulk values, the Fe-O-Fe bonding distance must increase, weakening the indirect exchange between Fe atoms and thus reducing the Néel temperature. Mismatch-induced strain has also been linked to a change of the critical temperature in cuprate superconductors (*13*).

PEEM spectromicroscopy is shown here to provide the necessary resolution and contrast to resolve the generally small (10 to 1000 nm) AFM domains in thin films. Our studies also open the door for combined linear and circular dichroism studies of the magnetic structure at ferromagnet-antiferromagnet interfaces (so-called exchange bias systems) that are both scientifically challenging and technologically important (*2, 25*).

References and Notes

1. J. B. Kortright *et al.*, *J. Magn. Magn. Mater.* **207**, 7 (1999).
2. J. Nogués and I. K. Schuller, *J. Magn. Magn. Mater.* **192**, 203 (1999).
3. W. L. Roth, *J. Appl. Phys.* **31**, 2000 (1960).
4. J. Baruchel, *Physica B* **192**, 79 (1993).
5. S. Saito, M. Miura, K. Kurosawa, *J. Phys. C: Solid State Phys.* **13**, 1513 (1980).
6. J. Stöhr *et al.*, *Phys. Rev. Lett.* **83**, 1862 (1999).
7. M. Fiebig, D. Frölich, G. Sluyterman v. L., R. V. Pisarev, *Appl. Phys. Lett.* **66**, 2906 (1995).
8. D. Spanke *et al.*, *Phys. Rev. B* **58**, 5201 (1998).
9. J. Stöhr, H. A. Padmore, S. Anders, T. Stammler, M. R. Scheinfein, *Surface Rev. Lett.* **5**, 1297 (1998).
10. S. Anders *et al.*, *Rev. Sci. Instrum.* **70**, 3973 (1999).
11. J. Stöhr *et al.*, *Science* **259**, 658 (1993).
12. J.-P. Locquet, A. Catana, E. Mächler, C. Gerber, J. G. Bednorz, *Appl. Phys. Lett.* **64**, 372 (1994).
13. J.-P. Locquet *et al.*, *Nature* **394**, 453 (1998).
14. H. McMurdie *et al.*, *Powder Diffr.* **1**, 269 (1986); S. E. Dann *et al.*, *J. Solid State Chem.* **109**, 134 (1994).
15. R. L. White, *J. Appl. Phys.* **40**, 1061 (1969).
16. High-resolution x-ray absorption measurements with

linear polarization were carried out with the spherical grating monochromator on the wiggler beam line 10.1 at the Stanford Synchrotron Radiation Laboratory (SSRL). Spectromicroscopy studies were carried out with the PEEM2 facility on beam line 7.3.1.1 at the Advanced Light Source (ALS) (*10*).

17. P. Kuiper, B. G. Searle, P. Rudolf, L. H. Tjeng, C. T. Chen, *Phys. Rev. Lett.* **70**, 1549 (1993).
18. D. Alders *et al.*, *Phys. Rev. B* **57**, 11623 (1998).
19. J. Lüning *et al.*, in preparation.
20. B. T. Thole, G. van der Laan, G. A. Sawatzky, *Phys. Rev. Lett.* **55**, 2086 (1985).
21. $\langle M^2 \rangle = S(S+1) + \langle M \rangle \coth(1/2\theta)$ with $\theta = -S(S+1)/3\langle M \rangle\, T/T_c$ in mean field approximation.
22. M. Eibschütz, S. Shtrikman, D. Treves, *Phys. Rev.* **156**, 562 (1967).
23. E. N. Abarra, K. Takano, F. Hellman, A. E. Berkowitz, *Phys. Rev. Lett.* **77**, 3451 (1996).
24. I. Lyubutin, T. Dimitrieva, A. Stepin, *J. Exp. Theor. Phys.* **88**, 590 (1999).
25. G. A. Prinz, *Science* **282**, 1660 (1998).
26. Supported by the Division of Chemical Sciences (SSRL) and the Division of Materials Science (ALS) of the Office of Basic Energy Sciences of the U.S. Department of Energy. J.W.S. and F.N. acknowledge support by the Swiss National Science Foundation. J.P.L. thanks I. K. Schuller for stimulating his interest in the exchange bias problem.

1 October 1999; accepted 15 December 1999

Molecules in a Bose-Einstein Condensate

Roahn Wynar, R. S. Freeland, D. J. Han, C. Ryu, D. J. Heinzen*

State-selected rubidium-87 molecules were created at rest in a dilute Bose-Einstein condensate of rubidium-87 atoms with coherent free-bound stimulated Raman transitions. The transition rate exhibited a resonance line shape with an extremely narrow width as small as 1.5 kilohertz. The precise shape and position of the resonance are sensitive to the mean-field interactions between the molecules and the atomic condensate. As a result, we were able to measure the molecule-condensate interactions. This method allows molecular binding energies to be determined with unprecedented accuracy and is of interest as a mechanism for the generation of a molecular Bose-Einstein condensate.

Bose-Einstein condensation of dilute atomic gases, first observed in 1995 (*1, 2*), has become a dynamic and wide-ranging field of research (*3*). Dilute gas condensates are similar in certain respects to previously studied systems such as superfluid liquid helium, but they also exhibit many qualitatively new features. Among the most important is that the atoms can bind together to form molecules. Molecular recombination in three-body collisions leads to atomic losses in Bose condensates (*4*), because molecular binding energy is converted into kinetic energy. However, it is also possible to form molecules coherently in a condensate through stimulated recombination in two-body collisions. In this case, the atoms and recombined molecules may form a two-species Bose-Einstein condensate consisting of both an atomic and a molecular component, and a very interesting class of coherent atomic and molecular matter wave phenomena is predicted to occur (*5–8*).

We now report molecular formation in a dilute gas Bose condensate through coherent stimulated recombination of atoms. Specifically, we created state-selected $^{87}Rb_2$ molecules by stimulated Raman free-bound transitions in an ^{87}Rb atomic condensate (*9*). The molecules were created with a negligible kinetic energy and a potential energy of the order of the chemical potential (~100 nK) of the atomic Bose condensate. We probed the molecules spectroscopically through measurements of the stimulated Raman transition rate. This rate displayed a resonance line shape with a width as small as 1.5 kHz and more than 10,000 times narrower than those of similar resonances previously measured in a laser-cooled gas (*10, 11*). This narrow width is a direct consequence of the vanishing kinetic energy spread of the Bose condensate, and it allowed us to measure the molecular binding energy with unprecedented accuracy. We found that the molecule-condensate interactions shift and broaden the transition resonance and, as a result, we could measure these interactions.

Cold molecules have been produced and detected previously through photoassociation of laser-cooled atoms (*12*). In contrast to our work here, these molecules were formed incoherently in many different ro-vibrational levels and had a relatively large kinetic energy spread on the order of 100 μK. Our work is more closely related to previous experimental studies of Feshbach resonances, which demonstrated dramatic modifications to the interactions between ultracold atoms (*13*). In such a resonance, a molecular level very near the dissociation limit plays a role as a transient intermediate state in a collision of two atoms. In principle, Feshbach resonances can lead to the same class of phenomena as the stimulated Raman free-bound coupling we explore here. In either kind of experiment, if the molecular level has a sufficiently long lifetime, its effect on the gas cannot be understood simply through the resonant modification of the two-body interaction. Instead, the molecules must be treated as a separate population with its own properties and interactions with the atomic gas. We realize this regime in our experiment.

Department of Physics, The University of Texas, Austin, TX 78712, USA.

*To whom correspondence should be addressed. E-mail: heinzen@physics.utexas.edu

The stimulated Raman process is illustrated in Fig. 1. The condensate is illuminated with two laser fields 1 and 2 of frequency ω_1 and ω_2, wavevector $\vec{k}_1$ and $\vec{k}_2$, and intensity I_1 and I_2, respectively. A close pair of atoms from the condensate in a continuum state $|f\rangle$ interacts through a potential $V_g(R)$. This pair simultaneously absorbs a photon from laser field 1, emits a photon into laser field 2, and undergoes a transition to a molecular bound state $|g\rangle$ of binding energy ε. The process becomes resonant when $\Delta\omega = \omega_2 - \omega_1 = \varepsilon$. This resonance condition is satisfied for only a single molecular ro-vibrational state, so only that state is formed. The momentum transferred from the photons to the molecule in this process is $\hbar(\vec{k}_1 - \vec{k}_2)$, and is almost exactly zero in our experiment, because the laser beams propagate in the same direction and have a very small frequency difference. Because the atoms in the condensate are almost perfectly at rest, the molecules are formed almost perfectly at rest inside the atomic condensate.

Our measurements were carried out in a Bose-condensed gas of $^{87}Rb\ 5^2S_{1/2}(f = 1, m_f = -1)$ atoms confined in a magnetic trap. Here, f and m_f give the total spin and spin projection quantum numbers of the atoms. Our method to produce a condensate is similar to that first demonstrated by Anderson *et al.* (*1*), and has been described previously (*14*). The atoms were first captured in an optical trap in a high vacuum and were laser-cooled, then were transferred to a magnetic "TOP" trap (*1*) and further cooled with radio frequency–induced evaporation. The number of atoms, the gas temperature, and the fraction of the atoms in the condensate were measured with a laser-absorption imaging technique. For highly evaporated clouds, we could produce a gas with a temperature below 130 nK, condensate fraction greater than 80%, condensate atom number $N_c = 3.6 \times 10^5$, and peak condensate density $n_0 = 2.7 \times 10^{14}\ cm^{-3}$ in a harmonic trapping potential $V_a(\vec{r}) = M\omega_r^2(x^2 + y^2)/2 + M\omega_z^2 z^2/2$, with $\omega_r/2\pi = 54$ Hz, $\omega_z/2\pi = 153$ Hz, and M the mass of an ^{87}Rb atom. We also produced condensates with a smaller atom number and density by continuing the evaporation further and by adiabatically lowering the trapping frequencies.

After the production cycle, we illuminated the condensate with the two laser fields for a period τ between 150 and 550 ms, with the trap left on. The TOP rotating magnetic field ampli-